JOURNAL OF CATALYSIS 132, 210–228 (1991)

Kinetics of the Hydrogen–Oxygen Reaction on Platinum

B. HELLSING,* B. KASEMO,* AND V. P. ZHDANOV†

*Department of Physics, Chalmers University of Technology, S-412 96 Göteborg, Sweden; and †Institute of Catalysis, Novosibirsk 630090, USSR

Received September 12, 1990; revised April 23, 1991

A kinetic model has been constructed primarily to describe the rates of water and hydroxyl desorption during the hydrogen–oxygen reaction on Pt at high temperatures, ~1000 K, and pressures in the range 1–1000 m Torr. The calculated results are compared with experimental observations. The model is based on dissociative sticking of H_2 and O_2 and hydrogen addition to oxygen to form OH. For water formation the two alternative routes $OH + H \rightarrow H_2O$ and $OH + OH \rightarrow H_2O + O$ are considered. OH decomposition, $OH \rightarrow O + H$, is found to be an important reaction step. Using available literature data and results from the model calculations, an enthalpy diagram for the reaction is constructed. It is concluded that a unique enthalpy diagram for the $H_2 + O_2$ reaction on Pt is still lacking, even at nearly zero coverage. Adsorbate–adsorbate interactions are expected to modify the enthalpy diagram at high coverages. The kinetic equations for various reaction steps have been formulated assuming random distribution of adsorbed species on a uniform surface. At fixed temperature, both routes for H_2O formation mentioned above can give a reasonably good quantitative description of the OH and H_2O desorption rates as functions of gas mixture and pressure in the regimes where experimental data are available. However, a closer analysis shows that the relative importance of the two water formation routes could depend sensitively on temperature and gas-phase H_2/O_2 ratio. High temperature and hydrogen excess favors the $OH + H \rightarrow H_2O$ route, while oxygen excess and low temperatures may favor the OH disproportionation reaction. The model has also been used to predict the reaction kinetics at high pressures up to 10^5 Torr. The latter results may be useful as guides to high-pressure experiments and in calculations of catalytic combustor performance.

1. INTRODUCTION

The kinetics of the hydrogen–oxygen reaction have been studied by many groups (see (*1–13*) and references therein). All authors agree that the dominant reaction is of the Langmuir–Hinshelwood type and occurs via one of the following steps for water formation

$$H^a + OH^a \rightarrow H_2O^a \quad (1.1)$$

$$OH^a + OH^a \rightarrow H_2O^a + O^a \quad (1.2)$$

$$H^a + H^a + O^a \rightarrow H_2O^a, \quad (1.3)$$

where the index a refers to adsorbed particles. Direct reactions involving molecular hydrogen or oxygen have not been confirmed. However, there are still several controversies or uncertainties concerning, e.g., (i) the relative importance of the different elementary reactions (1.1)–(1.3) above, (ii) the enthalpy diagram, and (iii) the magnitude of the activation energies for intermediate reaction steps. The reaction is known to be fast at room temperature and above. Chemisorbed oxygen and hydrogen react on Pt at temperatures as low as 120 K (*3, 4, 13*). For this reason, it is difficult to register intermediate particles in the reaction and discriminate a dominant route. OH species have been identified on the Pt surface only at low temperatures (around 100 K) using electron energy loss spectroscopy (EELS) (*12, 13*).

In our laboratory (in Sweden) the steady-state kinetics of H_2O and OH desorption from polycrystalline platinum have recently been studied (*7–11*) as a function of the

0021-9517/91 $3.00

relative hydrogen pressure, $\alpha = P_{H_2}/(P_{H_2} + P_{O_2})$. To obtain sufficient desorption rates of hydroxyl particles for detection by laser-induced fluorescence, the experiment must be performed at high temperatures (around 1000 K), otherwise the produced OH reacts to form H_2O before a measurable amount has time to desorb. The pressure was in the range 5–200 mTorr (1 Torr = 133 N m^{-2}). At lower temperatures and pressures $\leq$1 mTorr the hydroxyl signal measured by laser-induced fluorescence was too small for quantitative measurements. Further details of these experiments are found in Ref. (*10*).

The experimental data reported in Refs. (*7–11*) should make it possible to identify, in principle at least, the dominant routes of the hydrogen–oxygen reaction. The aim of the present work is to analyze and interpret the obtained results in detail by model calculations using the relevant published information on the hydrogen–oxygen reaction. This is the first complete presentation of the model used to analyze recent data (*11*). It is currently used as a guide and interpretation tool for ongoing and planned experiments on this reaction. The high-temperature regime of the reaction is emphasized.

In our analysis, step (1.3) is ignored because three-particle processes are usually considered to be negligible even at low temperatures. This step is definitely not important at high temperatures where the hydrogen coverage is low. Thus, our attention is focused on routes (1.1) and (1.2).

In comparison with Refs. (*7–11*), our understanding of the reaction kinetics has improved and we are now able to reproduce the experimental data better and in more detail. For example, including the decomposition reaction of adsorbed OH particles, additional features can be simulated such as the maximum production yields of OH^g and H_2O^g (index g refers to gas-phase particles) at their proper α-values, α_{OH} and α_{H_2O}, respectively. Also the "tail" of the production yield of OH^g at $\alpha > \alpha_{H_2O}$ (*7, 10*) is now reproduced. A major conclusion is that step (1.1) seems to be dominant at high temperatures and with not too small α-values, while step (1.2) may be dominant at large oxygen excess and/or low temperatures. The enthalpy diagram for the reaction is discussed and compared with other recent results. By comparison with data obtained at lower temperatures it appears that the enthalpy diagrams at high and low surface coverage look quite different. Using the obtained kinetic parameters, we have also extended the calculations to higher pressures (up to 10^5 Torr), where experimental data are as yet lacking. An efficient numerical method, used for solving the kinetic equations, is discussed.

2. KINETIC MODEL

The hydrogen–oxygen reaction on Pt is assumed to contain the following steps

$$H_2^g \rightleftarrows 2H^a \tag{2.1}$$

$$O_2^g \rightleftarrows 2O^a \tag{2.2}$$

$$H^a + O^a \rightleftarrows OH^a \tag{2.3}$$

$$H^a + OH^a \rightleftarrows H_2O^a \tag{2.4}$$

$$OH^a + OH^a \rightleftarrows H_2O^a + O^a \tag{2.5}$$

$$OH^a \rightarrow OH^g \tag{2.6}$$

$$H_2O^a \rightarrow H_2O^g. \tag{2.7}$$

We have assumed that the gas flow/pumping speed is sufficiently large to keep the H_2O partial pressure negligibly low; otherwise the reverse of (2.7) must be included. If the surface is uniform, the arrangement of adsorbed particles is random, and adsorption is competitive, this scheme results in the following steady-state kinetic equations

$$2S_{H_2}(\theta)F_{H_2} + k_{OH}^{dec}\theta_{OH}(1-\theta) + k_{H_2O}^{dec_1}\theta_{H_2O}(1-\theta) = 2k_{H_2}^{d}\theta_H^2 + k_{OH}^{f}\theta_H\theta_O + k_{H_2O}^{f_1}\theta_H\theta_{OH} \tag{2.8}$$

$$2S_{O_2}(\theta)F_{O_2} + k_{OH}^{dec}\theta_{OH}(1-\theta) + k_{H_2O}^{f_2}\theta_{OH}^2 = 2k_{O_2}^{d}\theta_O^2 + k_{OH}^{f}\theta_H\theta_O + k_{H_2O}^{dec_2}\theta_O \tag{2.9}$$

$$k^{f}_{OH}\theta_H\theta_O + k^{dec_1}_{H_2O}\theta_{H_2O}(1-\theta) + 2k^{dec_2}_{H_2O}\theta_{H_2O}\theta_O = k^{d}_{OH}\theta_{OH} + k^{dec}_{OH}\theta_{OH}(1-\theta) + k^{f_1}_{H_2O}\theta_H\theta_{OH} + 2k^{f_2}_{H_2O}\theta^2_{OH} \quad (2.10)$$

$$k^{f_1}_{H_2O}\theta_H\theta_{OH} + k^{f_2}_{H_2O}\theta^2_{OH} = k^{d}_{H_2O}\theta_{H_2O} + k^{dec_1}_{H_2O}\theta_{H_2O}(1-\theta) + k^{dec_2}_{H_2O}\theta_{H_2O}\theta_O, \quad (2.11)$$

where $F_i = AP_i\,(2\pi m_i T)^{-1/2}$ is the surface impingement rate of hydrogen ($i = H_2$) and oxygen ($i = O_2$), $A = 4$ Å^2 is the site area, P_i is the pressure, m_i is the mass of a molecule, $S_i(\theta)$ is the coverage-dependent sticking coefficient, and θ is the total surface coverage $0 \le \theta \le 1$. The Boltzmann constant is set to unity. The upper index in the rate constants refers to desorption (d), formation (f), or decomposition (dec). The subscripts 1 and 2 of f and dec refer to the two alternative H_2O formation/decomposition routes (2.4) and (2.5), respectively.

The OH and H_2O coverages on the Pt surface are usually small under reaction conditions even at quite low temperatures. At high temperatures, $T \ge 1000$ K, they are very small (except at large oxygen excess), and the hydrogen coverage is also low, as illustrated by the numerical results in Fig. 2. The surface is then predominantly covered by oxygen at oxygen excess in the gas mixture or is almost uncovered by oxygen at the hydrogen excess (except at the much higher pressures considered in Section 8).

In order to simulate the reaction kinetics at *high* coverages, we thus only need to know the dependence of various kinetic parameters on the oxygen coverage. The effect of oxygen on the hydrogen adsorption (sticking) probability is known to be rather weak (*2, 5*). Earlier (*5–11*), we have assumed that $S_{H_2} \sim (1-\theta)$. In the present study, the hydrogen sticking coefficient is treated as independent of coverage. The latter assumption results in a better agreement with the experimental measurements of the H_2O formation at oxygen excess.

The coverage dependence of the oxygen sticking coefficient is described (*5, 7, 10, 17*) by

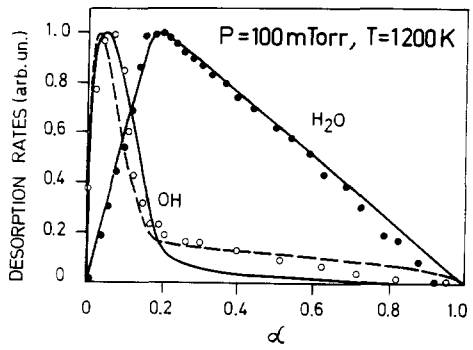

FIG. 1. H_2O and OH desorption rates as a function of the relative hydrogen pressure, $\alpha = P_{H_2}/(P_{H_2} + P_{O_2})$. The experimental data (*10*) for hydroxyl and water desorption are represented by open and solid circles, respectively. The solid and dashed lines are theoretical curves obtained by numerical solution to Eqs. (2.8)–(2.11) assuming that the reaction occurs only due to route (1.1) or route (1.2). Both routes yield the same results for H_2O production (solid line). In the case of OH desorption, the results for routes (1.1) (solid line) and (1.2) (dashed line) are somewhat different. The ratio of the maximum water and hydroxyl desorption rates is about 10^4. The temperature of the catalyst and the total H_2 and O_2 pressure are given in the figure.

$$S_{O_2}(\theta) = S_{O_2}(0)(1-\theta)^2. \quad (2.12)$$

The rate constants k^i_j are represented by the Arrhenius form

$$k^i_j = \nu^i_j \exp(-E^i_j/T). \quad (2.13)$$

The preexponential factors and activation energies for various reaction steps may be dependent on coverage due to lateral interactions between adsorbed particles or adsorbate-induced changes in the surface (*14*). Analyzing the kinetics of the OH desorption, we found it necessary to take into account a *possible* coverage dependence of the activation energy for this step. The reason is that without such a dependence the reaction step OH + OH → H_2O + O (2.5) could never account for the data of Fig. 1, since it implies a coincidence of the H_2O and OH desorption maxima. However, with a coverage-dependent OH desorption energy this condition is relaxed. To the lowest order

with respect to coverage, we have

$$E^{d}_{OH}(\theta) = E^{d}_{OH}(0) - B\theta, \qquad (2.14)$$

where B is a constant and $E^{d}_{OH}(\theta)$ the activation energy for OH desorption at coverage θ. The main effect of B is that it influences the position and intensity of the OH desorption maximum with respect to the H_2/O_2 mixing ratio. A positive B-value shifts the OH maximum to more oxygen-rich mixtures. The coverage dependence of the activation energy of other reaction steps has been ignored because inclusion of such effects does not result in new qualitative features in the calculated kinetics of OH desorption (*15*). Moreover, no information is available at present on coverage-dependent activation energies for intermediate steps.

The preexponential factors for various processes are assumed to be independent of coverage. The values of the preexponential factors can be estimated using the elementary collision theory (*7*) or the transition state theory (*15*). All preexponential factors have been taken to be 10^{13} s^{-1}.

Several of the simplifications made above could be questioned, for example, the assumption of constant preexponential factors 10^{13} s^{-1}, the coverage independence of all the activation energies (except one), use of the same $S_{O_2}(\theta)$ independent of whether θ is composed of hydrogen or oxygen. The main motivations for the simplifications are as follows. (i) Because there is still lack of knowledge of the quantitative values of several kinetic constants, we emphasize the qualitative or semiquantitative understanding of the $H_2 + O_2$ reaction, over a perfect quantitative agreement between calculation and experimental data. (ii) We therefore keep the number of parameters as low as possible. (iii) The limited range of temperatures over which quantitative comparison is made between calculated and experimental results motivates the omission of the T-dependence of the preexponential factors. (iv) No detailed information is available on how the sticking of O_2 depends on H coverage, and the H coverage is always low in the T, P regime where we compare with experimental data.

It is obvious that these simplifications signal caution when extrapolations are made from the calculations to, e.g., pressure–temperature regimes outside the main target regime of this work (1–100 mTorr, 800–1300 K).

3. H_2O FORMATION: GENERAL FEATURES

To evaluate the relative importance of the two routes of the hydrogen–oxygen reaction, the kinetics of H_2O and OH desorption were analyzed numerically, assuming that the reaction occurs only due to route (1.1) or only due to route (1.2), respectively. In the former case, step (2.5) was ignored, and in the latter case, step (2.4) was omitted. The corresponding results are presented in Sections 4 and 5. Before discussing these results, it is appropriate to review briefly some general features of the steady-state kinetics of water formation (*5–11*).

The hydrogen–oxygen reaction is very fast at the high temperatures considered here. This has two important consequences. First, the oxygen and hydroxyl desorption rates are negligible in comparison with the formation and desorption rates of H_2O (except at very low relative hydrogen concentrations $\alpha < 0.05$). Second, the surface is covered predominantly by oxygen in the oxygen excess regime, i.e., when

$$2S_{O_2}(0)F_{O_2} > S_{H_2}(0)F_{H_2}, \qquad (3.1)$$

and the surface is almost uncovered, $\theta \ll 1$, in the hydrogen excess regime, i.e., when

$$2S_{O_2}(0)F_{O_2} < S_{H_2}(0)F_{H_2}. \qquad (3.2)$$

In the former case, the hydrogen desorption rate is negligible and the reaction kinetics are described by the equation

$$2S_{O_2}(\theta)F_{O_2} = S_{H_2}(\theta)F_{H_2}. \qquad (3.3)$$

In the latter case, the hydrogen desorption compensates the hydrogen excess and we have

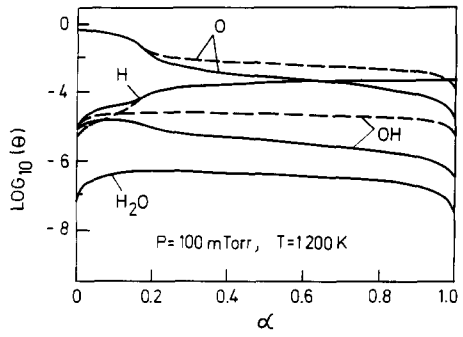

FIG. 2. Coverages of adsorbed species for the case presented in Fig. 1. Solid and dashed curves have been obtained by numerical solution to Eqs. (2.8)–(2.11) for routes (1.1) and (1.2), respectively. Both routes yield the same results for the H_2O coverage. Note the rapid variation with α in the H, O, and OH coverages around the rate maximum for water formation, $\alpha \approx 0.2$.

$$2S_{O_2}(0)F_{O_2} + k^d_{H_2}\theta_H^2 = S_{H_2}(0)F_{H_2}. \quad (3.4)$$

The rate of water production is in both cases equal to twice the rate of oxygen adsorption

$$r^f_{H_2O} = 2S_{O_2}(\theta)F_{O_2} \quad (3.5)$$

as long as oxygen and OH desorption is negligible.

The description of the water formation rate is thus the same for both possible routes (2.4) and (2.5) of the reaction. In particular, for both routes we have the following.
(i) The rate of water formation has its maximum when

$$2S_{O_2}(0)F_{O_2} = S_{H_2}(0)F_{H_2}. \quad (3.6)$$

(ii) The relative hydrogen pressure, α_{H_2O}, at the maximum water formation is independent of the total pressure.
(iii) The rate of water formation is proportional to the total pressure.
Conditions (i)–(iii) hold as long as $\theta \ll 1$ and as long as all desorption rates, except H_2O desorption, are negligible which for $\alpha \approx \alpha_{H_2O}$ is fulfilled up to very high pressures (see Section 8) and is valid even for the high temperatures considered here (except for very small α-values).

These analytical predictions are in agreement with the numerical results obtained by solving Eqs. (2.8)–(2.11) and with the experimental data obtained at P = 5–200 mTorr (see Figs. 1–4). Only at much higher pressures will conclusions (i)–(iii) change.

An interesting observation is that Eqs. (3.5) and (3.6) can be employed to determine the sticking coefficients for H_2 and O_2 *under reaction conditions* using the experimentally measured dependence of the water formation rate on α. In particular, in measuring the maximum water production rate and the corresponding α-value at a given total pressure, it is possible to evaluate the oxygen sticking coefficient using Eq. (3.5). The ratio of the surface impingement rates of hydrogen and oxygen at maximum water production can then be used (see Eq. (3.6)) to calculate the hydrogen sticking coefficient at low coverages. In this way, $S_{O_2}(0) = 0.02$ and $S_{H_2}(0) = 0.05$ were determined at T =

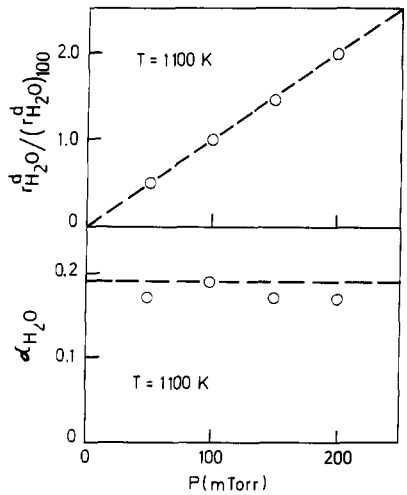

FIG. 3. The maximum desorption rate of water (upper panel) and the corresponding relative hydrogen pressure (lower) as a function of the total pressure. The experimental data (*10*) are represented by empty circles. The dashed lines are theoretical curves obtained by numerical solution to Eqs. (2.8)–(2.11) assuming that the reaction occurs only due to route (1.1) or (1.2). Both routes yield the same results. Experimental and calculated H_2O desorption rates are normalized independently to the value at P = 100 mTorr, $(r^d_{H_2O})_{100}$.

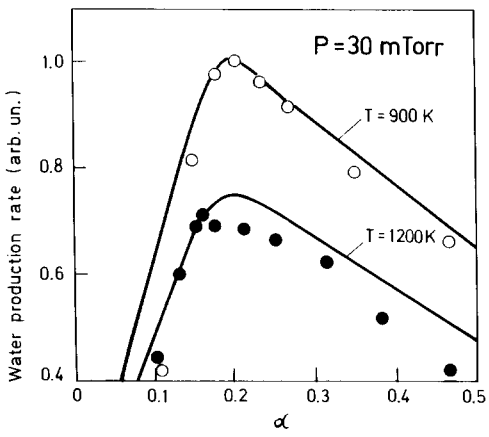

FIG. 4. H_2O desorption rate as a function of the relative hydrogen concentration at $T = 900$ and 1200 K. The experiment data (*10*) are represented by open circles. The solid lines are theoretical curves obtained by numerical solution to Eqs. (2.8)–(2.11) assuming that the temperature dependence of the H_2 and O_2 sticking coefficients is described by Eq. (3.7). Experimental and calculated results are normalized independently to the maximum desorption rate at $T = 900$ K. The theoretical results are the same for routes (1.1) and (1.2).

1100 K (*10*). These values have been employed to fit the experimental data by solving Eqs. (2.8)–(2.11).

(Parenthetically, we note that the temperature dependence of the sticking coefficients can be estimated studying the dependence of the absolute value of the water formation rate and of α_{H_2O} on temperature. The experiments show (Fig. 4) that in this high-temperature regime α_{H_2O} is almost independent of temperature. This means that the temperature dependence of the hydrogen and oxygen sticking coefficients is about the same. On the other hand, the observed decrease in the maximum water production rate with increasing temperature can be explained by a decrease in both sticking coefficients with temperature rise. The experimental data can be fitted (Fig. 4) assuming the following temperature dependence of the oxygen and hydrogen sticking coefficients

$$S(T) = S_0 T_0/T, \tag{3.7}$$

where S_0 is the sticking coefficient at $T = T_0$. On closer inspection, however, the oxygen sticking coefficient seems to decrease somewhat faster than the hydrogen sticking coefficient with increasing temperature. The latter conclusion derives from the slight decrease of α_{H_2O} with the temperature increase (see Fig. 4 in this work or Fig. 11 in Ref. (*10*).)

4. OH DESORPTION, ROUTE (1.1)

The kinetics of OH desorption is more sensitive than the H_2O production to details of the reaction mechanism. Let us first consider the kinetics of OH desorption assuming that reaction step (2.4) is dominant and neglecting step (2.5). We then treat the opposite case.

For hydrogen excess, $\alpha > \alpha_{H_2O}$, the surface is almost uncovered and the hydrogen coverage, defined by Eq. (3.4) is

$$\theta_H = [(S_{H_2}(0)F_{H_2} - 2S_{O_2}(0)F_{O_2})/k^d_{H_2}]^{1/2}. \tag{4.1}$$

Neglecting the water decomposition reaction (2.5) and using Eq. (3.5), we have

$$r^f_{H_2O} = 2S_{O_2}(0)F_{O_2} = k^f_{H_2O}\theta_H\theta_{OH}. \tag{4.2}$$

Equations (4.1) and (4.2) yield the following expression for the OH desorption rate

$$r^d_{OH} \equiv k^d_{OH}\theta_{OH} = \frac{2k^d_{OH}S_{O_2}(0)F_{O_2}[k^d_{H_2}]^{1/2}}{k^f_{H_2O}[S_{H_2}(0)F_{H_2} + 2S_{O_2}(0)F_{O_2}]^{1/2}}. \tag{4.3}$$

The apparent order of OH desorption with respect to the total pressure is seen to be $\frac{1}{2}$ and the apparent activation energy ε^d_{OH} of the process is different from the true activation energy for OH desorption (*9*).

$$\varepsilon^d_{OH} = E^d_{OH} - E^f_{H_2O} + E^d_{H_2}/2. \tag{4.4}$$

Using the experimental value of ε^d_{OH} and Eq. (4.4), E^d_{OH} was recently determined to be $E^d_{OH} = 2.0$ eV (*11*). Note that the latter value corresponds to the low-coverage limit (i.e., no adsorbate–adsorbate interaction) and assumes route (1.1) to be the dominant one. As shown in the next paragraph, route (1.2)

can only give good agreement with the experimental data if considerable adsorbate–adsorbate interaction is assumed for small α (= high coverage of oxygen).

For oxygen excess, the surface is predominantly covered by oxygen, the oxygen coverage is essentially independent of the total pressure (see Eq. (3.3)), and the reaction rate (see Eq. (3.5)) is

$$r^{f}_{H_2O} = 2S_{O_2}(\theta_O)F_{O_2} = k^{f_1}_{H_2O}\theta_H\theta_{OH}. \quad (4.5)$$

Assuming equilibrium between formation and decomposition of OH radicals (this assumption is justified because the OH decomposition is a rapid process even in comparison with the H_2O formation as long as $\theta_H \ll 1$), we have

$$k^{f}_{OH}\theta_H\theta_O = k^{dec}_{OH}\theta_{OH}(1 - \theta_O). \quad (4.6)$$

Equations (4.5) and (4.6) yield

$$r^{d}_{OH} \equiv k^{d}_{OH}\theta_{OH} = \frac{k^{d}_{OH}[2S_{O_2}(\theta_O)F_{O_2}k^{f}_{OH}\theta_O]^{1/2}}{[k^{f_1}_{H_2O}k^{dec}_{OH}(1 - \theta_O)]^{1/2}}. \quad (4.7)$$

The apparent order of OH desorption with respect to the total pressure is again $\frac{1}{2}$ (since θ_O is independent of pressure), while the apparent activation energy is

$$\varepsilon^{d}_{OH} = E^{d}_{OH} + (E^{f}_{OH} - E^{dec}_{OH} - E^{f_1}_{H_2O})/2. \quad (4.8)$$

In deriving Eqs. (4.1)–(4.7) we have assumed that desorption of OH and oxygen is negligible in comparison with water production. This seems to be justified as long as $\alpha > 0.05$. Equations (4.4) and (4.8) show that the apparent activation energy ε^{d}_{OH} varies with α even if E^{d}_{OH} is constant (*9*), which is also observed in the experiment (11).

To describe the kinetics of OH desorption in more detail, we need to know the activation energies of various reaction steps. Some of them ($E^{d}_{H_2}$, $E^{d}_{O_2}$, and $E^{d}_{H_2O}$) are known from the literature (see Table 1). $E^{d}_{OH}(O)$ has been estimated above and in Ref. (*11*). (A larger value reported recently (*31*) is discussed later.) Our analysis has also

TABLE 1

Activation Energies (eV) and Sticking Coefficients at Zero Coverage Used in the Model Calculations

Activation energies (eV)		Ref.
$E^{d}_{H_2}$	0.70	(*20*)
$E^{d}_{O_2}$	2.50	(*21*)
E^{f}_{OH}	0.35	(*22*)
E^{d}_{OH}	2.00 or 2.20	
$E^{d}_{H_2O}$	0.42	(*18*)
$E^{f_1}_{H_2O}$	0	
$E^{f_2}_{H_2O}$	0	
Sticking coefficients		**Ref.**
$S_{H_2}(0)$	0.05	(*23*)
$S_{O_2}(0)$	0.02	(*23*)

$E^{dec}_{OH} = E^{f}_{OH} + E^{d}_{OH} - \Delta E_{OH} - \frac{1}{2}(E^{d}_{H_2} + E^{d}_{O_2})$

$E^{dec_1}_{H_2O} = E^{d}_{H_2O} + E^{f_1}_{H_2O} - \frac{1}{2}E^{d}_{H_2} - E^{d}_{OH} + \Delta E_{OH} + \Delta E_{H_2O}$

$E^{dec_2}_{H_2O} = E^{d}_{H_2O} + E^{f_2}_{H_2O} - \frac{1}{2}E^{d}_{O_2} - 2E^{d}_{OH} + 2\Delta E_{OH} + \Delta E_{H_2O}$

$\Delta E_{OH} = \frac{1}{2}(D^{d}_{H_2} + D^{d}_{O_2}) - D^{d}_{OH}$

$S_{H_2}(\theta) = S_{H_2}(0)$

$S_{O_2}(\theta) = S_{O_2}(0)(1 - \theta)^2$

Note. $\Delta E_{H_2O} = 2.5$ eV is the heat of formation of water in gas phase. D_{H_2}, D_{O_2}, and D_{OH} are gas-phase dissociation energies of hydrogen, oxygen, and hydroxyl, respectively.

shown that in the case of route (1.1) good agreement with the experimental data for OH desorption can be obtained employing no or only weak coverage dependence of the activation energy for OH desorption (11). In the calculations presented below we have, however, used Eq. (2.14) with $B = 0.2$ eV, because this gives a slight improvement of the r^{d}_{OH} vs a curve in comparison with the case $B = 0$. Almost the same results are obtained, however, if the coverage dependence of E^{d}_{OH} is neglected. When the alternative route (1.2) for water formation is considered the situation is very different and a coverage-dependent E^{d}_{OH} is vital for obtaining agreement between experiment and theory (see below). (Remember that we are treating the two different routes in an "either or" manner. As discussed below, a

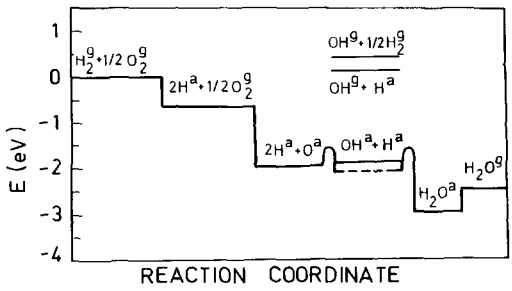

FIG. 5. Enthalpy diagram for the hydrogen–oxygen reaction on platinum. The activation energies for the reaction steps are chosen according to Table 1 and discussed in the text. The solid and dashed lines for the $OH^a + H^a$ energy level correspond, respectively, to $E^d_{OH}(0) = 2$ eV (route (1.1)) and 2.2 eV (route (1.2)).

combination of them would probably give the best overall description for all conditions of pressure, temperature, and mixing ratio.)

The activation energy for OH formation is assumed <0.35 eV, since the water formation reaction can proceed down to ~140 K at a reasonable rate (*3, 4*). On the other hand, we assume that the condition $E^f_{OH} \geq E^{diff}_H$, where E^{diff}_H is the activation energy for surface diffusion of hydrogen, holds for OH formation. For H/Pt(111) at about T = 200 K, E^{diff}_H has been reported to be 0.5 eV in the limit of zero coverage (*27*). This relatively large value of E^{diff}_H is due to the presence of steps on the Pt(111) surface. For a perfect Pt(111) surface we expect E^{diff}_H to be considerably smaller. For example George *et al.* and Mullins *et al.* (*27b*) have reported the values $E^{diff}_H = 0.17$ and 0.15 eV, respectively, for H/Ni(100). We have employed $E^f_{OH} = 0.35$ eV, which we regard as an upper limit of E^f_{OH}.

Using the available experimental data, we have constructed an enthalpy diagram for the reaction which is discussed later (Fig. 5). Employing this diagram, one can easily calculate E^{dec}_{OH} and $E^{dec}_{H_2O}$ (see also Table 1). In particular, $E^{dec}_{H_2O}$ is expressed through $E^f_{H_2O}$. The consequences of relaxing the condition $E^f_{OH} \leq 0.35$ eV and employing larger values of E^f_{OH} and $E^f_{H_2O}$, as in the recent work by Anton and Cadogan (*31*), are discussed in Sections 6 and 7.

An important conclusion from the enthalpy diagram is that the OH decomposition is a fast and important process for the overall kinetics. Thus, this step should always be taken into account in the calculations. (In previous publications (*5, 7, 9, 11*), the OH decomposition was neglected, which caused some disagreement between theory and experiment, e.g., a too-high desorption yield of OH in the calculations (*7, 9, 11*)).

Using the input parameters presented in Table 1 and in the previous sections, we solved Eqs. (2.8)–(2.11) numerically employing the multidimensional Newton–Raphson method (see Appendix). Results of the calculations are shown in Figs. 1–4 and 6–7. Route (1.1) for H_2O formation is seen to give a good quantitative description of the experimental data (*7, 10*) for H_2O and OH production over the whole range of gas mixtures, α, at pressures ~1–100 mTorr and temperatures 900–1200 K. Route (1.1) reproduces the shape of $r^d_{H_2O}$ vs α. The peak position and height come out correctly because they are determined by $S_{H_2}(0)$ and $S_{O_2}(0)$, which are determined from experi-

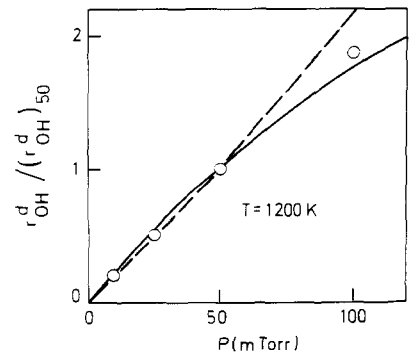

FIG. 6. The maximum OH desorption rate as a function of the total pressure. The experimental data (*10*) are represented by open circles. The solid and dashed lines are theoretical curves calculated, respectively, for routes (1.1) and (1.2). Experimental and calculated results are normalized independently to the desorption rate at P = 50 mTorr, $(r^d_{OH})_{50}$.

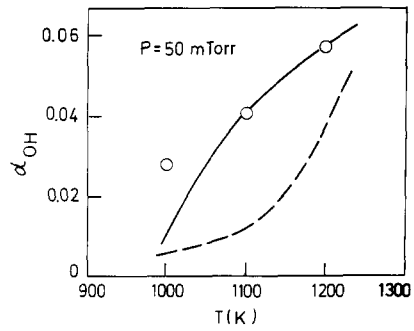

FIG. 7. Relative hydrogen concentration corresponding to the maximum OH desorption as a function of temperature. The experimental data (*10*) are represented by empty circles. The solid and dashed lines are theoretical curves calculated, respectively, for routes (1.1) and (1.2).

ments as described earlier. It also reproduces correctly the major shape of the r^{d}_{OH} vs α-curve and its peak position and absolute value. The slight difference in peak widths in the measured and calculated OH curves may be caused by too-simple coverage dependences in $S_{H_2}(\theta)$, $S_{O_2}(\theta)$, and $E^{d}_{OH}(\theta)$ in the regime where the oxygen coverage is high. Furthermore, the P-dependences of $r^{d}_{H_2O}$, α_{H_2O}, and r^{d}_{OH} are reasonably well reproduced over the P-range where experimental data are available (*11*) (see Figs. 3 and 6). Also the T-dependence of α_{OH} (and r^{d}_{OH}) and the α-dependence of the apparent activation energy for OH desorption are reproduced as demonstrated in Figs. 7 and 8 and in a separate analysis (*11*).

The presented numerical results for OH desorption were obtained assuming $E^{f_1}_{H_2O} = 0$ but essentially the same results occur for all values of $E^{f_1}_{H_2O} < 0.2$ eV. However, if $E^{f_1}_{H_2O} > 0.2$ eV, the description of the kinetics of OH desorption is poorer (if $E^{f}_{OH} \leq 0.35$ eV). Thus, if route (1.1) is dominant, the upper limit value of $E^{f_1}_{H_2O}$ seems to be 0.2 eV. On the other hand, the condition $E^{f_1}_{H_2O} \geq E^{diff}_{H}$ must hold for step (1.1). Using the same argument as for E^{f}_{OH}, that $E^{f_1}_{H_2O}$ should reflect that H_2O formation proceeds at a reasonable rate down to 140 K, one arrives at an upper limit of $E^{f_1}_{H_2O}$ of about 0.35 eV.

At this point, it is appropriate to discuss some differences between the kinetic model described here and the one employed in the earlier analysis of experimental data (*7*, *10*) and in the study of kinetic effects on the apparent activation energy for OH desorption (*9*). The improvement of the model consists of (i) inclusion of the OH decomposition reaction OH → O + H, (ii) a sticking coefficient for H_2, which is independent of oxygen coverage, (iii) explicit inclusion of the H_2O coverage and the reverse reaction (2.5), and finally (iv) inclusion of the alternative H_2O production route (1.2) (see Section 5).

These changes were partly motivated by some discrepancies between the results of the earlier model calculations and the more recent experimental data (*10*). For example, the OH "tail" (Fig. 1) at higher α-values (increasing H_2 concentration) beyond the OH maximum was not reproduced by the early model (*7*) and the absolute intensity of the OH desorption flux (and thus also the OH coverage) was too high. Both these problems were resolved by inclusion of OH decomposition. The latter also resulted in much better agreement between the experimentally observed and calculated pressure dependences of the OH desorption rate. The

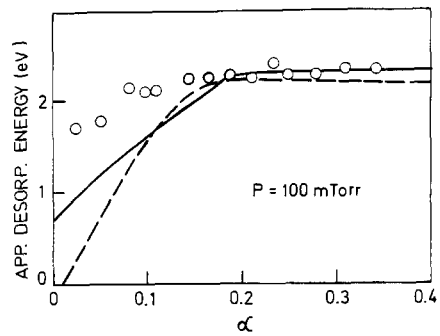

FIG. 8. The apparent activation energy for OH desorption as a function of the relative hydrogen pressure. The experimental data (*10*) are represented by open circles. The solid and dashed lines are theoretical curves calculated, respectively, for routes (1.1) and (1.2).

inclusion of the OH decomposition step results in a reduction in the OH coverage (by about two orders of magnitude), and consequently raises the O and H coverages. Therefore the rapid change (Fig. 2) in these coverages around the critical point $\alpha = \alpha_{H_2O}$, corresponding to the water desorption rate maximum, is smaller when OH decomposition is included than when it is omitted.

The change in the employed coverage dependence of the H_2 sticking coefficient, $S_{H_2}(\theta)$, from $(1 - \theta_O)$ dependence (*7*) to a coverage-independent sticking, was motivated as follows. The $(1 - \theta_O)$ factor in combination with second-order adsorption for O_2 produces a faster than linear increase in $r^d_{H_2O}$ with increasing α for the smallest α-values (see (*7*, Fig. 3)) while the improved experimental data (*10*) show a linear increase. The latter is reproduced by the model if a coverage-independent sticking coefficient for hydrogen is used. Also several observations reported in the literature support a coverage-insensitive H_2 sticking coefficient even at large oxygen coverages (*2*). The weak dependence of the hydrogen sticking coefficient on oxygen coverage could be due to a precursor mechanism of hydrogen adsorption on the oxygen-covered surface. It must be admitted, however, that the employed forms of both $S_{H_2}(\theta)$ and $S_{O_2}(\theta)$ are probably only approximations to more complex coverage dependences where also the surface microstructure, defects, etc., are involved.

Finally, the explicit inclusion of the H_2O coverage, although it is very small, was motivated by the observation that OH may be produced via the reaction $H_2O^a + O^a \rightarrow 2OH^a$ (*8*). Thus, in order to account correctly for the measured OH desorption rate, this reaction step may sometimes have to be considered. We found, however, that the calculated OH desorption rates at all α-values are dominated by OH produced by the forward reaction (2.3) and that only minor (but measurable) contributions come from the water decomposition reactions (2.4) or (2.5). The main reason is that the H_2O coverage is always so low that the last two terms of Eq. (2.11) become very small. Furthermore, the activation energies for the decomposition reactions (2.4) and (2.5) are relatively large (Fig. 5). An additional reason for the inclusion of the water coverage was to make possible analysis of recent experimental results from the $H_2O + \frac{1}{2}O_2 \rightarrow 2OH$ reaction (*33*).

5. OH DESORPTION, ROUTE (1.2)

Let us now consider the OH desorption kinetics assuming reaction step (2.5) to be dominant and neglecting step (2.4). In this case, the rate of water formation is (cf. Eq. (3.5))

$$r^f_{H_2O} = 2S_{O_2}(\theta)F_{O_2} = k^{f_2}_{H_2O}\theta^2_{OH}. \quad (5.1)$$

Using this equation, we obtain the following expression for the rate of OH desorption

$$r^d_{OH} \equiv k^d_{OH}\theta_{OH} = k^d_{OH}[2S_{O_2}(\theta)F_{O_2}/k^{f_2}_{H_2O}]^{1/2}. \quad (5.2)$$

The apparent order of OH desorption with respect to the total pressure is again seen to be $\frac{1}{2}$. The apparent activation energy is now

$$\varepsilon^d_{OH} = E^d_{OH} - E^{f_2}_{H_2O}/2. \quad (5.3)$$

The experiment yields $\varepsilon^d_{OH} = 2.2$ eV at hydrogen excess (11). With $E^{f_2}_{H_2O} = O$ in Eq. (5.3), we obtain $E^d_{OH} = 2.2$ eV, to be compared with the value 2.0 eV when the reaction step (2.4) was considered. Both values correspond to the low coverage limit.

To fit the experimental data, we solved Eqs. (2.8)–(2.11) using $E^d_{OH}(O) = 2.2$ eV and the same values of $E^d_{H_2}, E^d_{O_2}$, and $E^d_{H_2O}$ as in the case of route (1.1). The activation energies E^{dec}_{OH} and $E^{dec_2}_{H_2O}$ were calculated using these values (see Table 1) and employing the enthalpy diagram (Fig. 5). The activation energy $E^{f_2}_{H_2O}$ was set to zero. However, about the same results were obtained for $E^{f_2}_{H_2O} \leq 0.2$ eV.

The OH desorption yield vs α (Fig. 1) cannot be reproduced by route (1.2) alone

unless a relatively large repulsive hydroxyl–oxygen interaction is assumed. A value of $B = 0.7$ eV in Eq. (2.14) is necessary to bring the maximum in the OH desorption yield (Fig. 1) to the experimental α-value. With no such repulsive interaction the maximum in the OH and H_2O desorption yields will always coincide in route (1.2) (which is easily seen by comparing Eqs. (5.1) and (5.2)).

The results of these calculations are presented in Figs. 1–4, 6, and 7. For the H_2O production, route (1.2) yields just the same result as route (1.1). If the temperature is kept fixed, route (1.2) also reproduces most features of the kinetics of OH desorption. Neither of these two observables, therefore, can be used to discriminate unambiguously between routes (1.1) and (1.2) (unless the large B-value for route (1.2) is considered unrealistically large). However, the temperature dependence of the kinetics of OH desorption is more poorly reproduced by route (1.2) in comparison with route (1.1) (see Figs. 7 and 8). Thus, route (1.1) seems to be dominant in the hydrogen–oxygen reaction, at least at high temperatures and not too small α-values (see below). We cannot exclude route (1.2) at low T and/or small α.

Some experimental data pointing in favor of route (1.2) on Pt are the following. At low temperatures, the water formation on Pd has been shown to proceed via $OH^a + OH^a \rightarrow H_2O^a + O^a$ (*24*), and there are indications that this scheme holds also on Pt (*2, 8*). EELS results of coadsorbed water and oxygen demonstrate production of OH on several of the Pt group metals (*18, 19*). This is attributed to the reaction $H_2O^a + O^a \rightarrow 2\,OH^a$. LIF experiments with H_2O/O_2 mixtures also demonstrate production of OH desorbing from the surface of Pt (*8, 33*). However, in this case it is also shown (*33*), using the kinetic model described here, that the OH production can be accounted for by the reverse reaction route (2.4), i.e., $H_2O \rightarrow OH + H$. The latter route is actually favored when results from H_2O formation and decomposition are compared (*33*).

6. COMPARING ROUTES (1.1) AND (1.2)

In the previous sections, we have shown that both routes (1.1) and (1.2) can give a good quantitative description of the kinetics of OH and H_2O desorption. However, route (1.2) requires a relatively strong coverage dependence of the OH desorption energy in order to reproduce the data for all α-values. This strong coverage dependence is somewhat questionable in view of recent results (*33*) for OH formation in H_2O/O_2 mixtures at the same temperatures and pressures as those considered here. These results could only be reconciled with route (2.5) if $B \leq 0.05$. It is of continuing interest to investigate in which parameter regimes one or the other route may be dominant.

For routes (1.1) and (1.2), the reaction rate is, respectively, represented by $r^{f_1}_{H_2O} = k^{f_1}_{H_2O}\theta_H\theta_{OH}$ and $r^{f_2}_{H_2O} = k^{f_2}_{H_2O}\theta^2_{OH}$. Thus, route (1.1) is dominant if

$$\gamma \equiv r^{f_1}_{H_2O}/r^{f_2}_{H_2O} = k^{f_1}_{H_2O}\theta_H/(k^{f_2}_{H_2O}\theta_{OH}) > 1. \quad (6.1)$$

Using Eqs. (4.1) and (4.2), we can rewrite condition (6.1) at hydrogen excess as

$$\gamma = \frac{(k^{f_1}_{H_2O})^2[S_{H_2}(0)F_{H_2} - 2S_{O_2}(0)F_{O_2}]}{k^{f_2}_{H_2O}k^{d}_{H_2}2S_{O_2}(0)F_{O_2}} > 1. \quad (6.2)$$

This condition is always fulfilled for α sufficiently close to unity, i.e., at *large hydrogen excess where consequently route (1.1) must dominate*. Let us then consider α-values not too far from the water maximum, namely

$$[S_{H_2}(0)F_{H_2} - 2S_{O_2}(0)F_{O_2}]/[2S_{O_2}(0)F_{O_2}] \approx 1, \quad (6.3)$$

which corresponds to $\alpha \approx 2\alpha_{H_2O}$. Using relationship (6.3), we can simplify Eq. (6.2) as

$$(k^{f_1}_{H_2O})^2/(k^{f_2}_{H_2O}k^{d}_{H_2}) > 1. \quad (6.4)$$

Setting $\nu^{f_1}_{H_2O} = \nu^{f_2}_{H_2O} = \nu^{d}_{H_2}$, we may rewrite Eq. (6.4) as

$$2E^{f_1}_{H_2O} < E^{f_2}_{H_2O} + E^{d}_{H_2}. \quad (6.5)$$

We arrived earlier at $E^{f_1}_{H_2O} < 0.2$ eV and $E^{f_2}_{H_2O} < 0.2$ eV. Equation (6.5) is thus likely to be fulfilled since $E^{d}_{H_2}$ is 0.7–0.8 eV. We repeat that Eq. (6.5) was derived assuming that hydrogen is in slight excess. (Note that as long as $E^{f_1}_{H_2O} < E^{d}_{H_2}/2 \approx 0.35$ route 1.1 dominates at all hydrogen excess concentrations even if $E^{f_2}_{H_2O} = 0$).

Using Eq. (4.6), one can rewrite condition (6.1) for oxygen excess as

$$\gamma = (1 - \theta_O)k^{f_1}_{H_2O}k^{dec}_{OH}/(\theta_O k^{f_2}_{H_2O}k^{f}_{OH}) > 1. \quad (6.6)$$

We see that route (1.2) may become dominant as $\theta_O \to 1$ (oxygen excess), even if route (1.1) is dominant at $\theta_O \to 0$ (hydrogen excess). For example, at $\theta_O \approx 0.5$ and setting $\nu^{f_1}_{H_2O} = \nu^{f_2}_{H_2O} = \nu^{dec}_{OH} = \nu^{f}_{OH}$ and $\theta_O \approx 0.5$, we can replace Eq. (6.6) by

$$E^{f_1}_{H_2O} + E^{dec}_{OH} < E^{f_2}_{H_2O} + E^{f}_{OH}. \quad (6.7)$$

A somewhat more detailed analysis of γ in the oxygen excess regime $0.05 < \alpha < 0.20$ is shown in Fig. 10. Using Eq. (3.3) and the experimentally determined $S_{O_2}(0)/S_{H_2}(0)$ we obtain the α-dependence of θ_O,

$$\theta_O(\alpha) = 1 - 2\sqrt{\frac{\alpha}{1-\alpha}}, \quad (6.8)$$

by which we obtain, by use of Eq. (6.6), $\gamma(\alpha)$ analytically for any set of values of E^{d}_{OH}, $E^{f_1}_{H_2O}$, and $E^{f_2}_{H_2O}$. Figure 10 shows that for a variety of reasonable parameter choices there is a crossing from a route (1.1)-dominated reaction to a route (1.2)-dominated reaction as α becomes small. The exact crossing point where the two routes contribute equally varies with the choice of parameters.

The relative importance of the two routes, i.e., the value of γ, also varies with temperature. The values of the involved activation energies are such that, at a given α-value, one route may be dominant at high temperatures and the other at low temperatures.

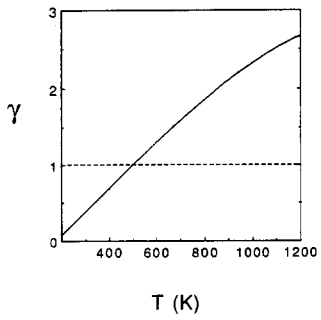

FIG. 9. Parameter γ as a function of temperature: γ is the ratio of the two water production rates resulting from the alternative mechanisms OH + H → H_2O and OH + OH → H_2O + O, respectively. The curve has been calculated according to Eq. (6.2) assuming $\nu^{f_1}_{H_2O} = \nu^{f_2}_{H_2O} = \nu^{d}_{H_2}$, $2E^{f_1}_{H_2O} - E^{f_2}_{H_2O} - E^{d}_{H_2} = 0.07$ eV and $[S_{H_2}(0)F_{H_2} - 2S_{O_2}]/[2S_{O_2}(0)F_{O_2}] = 5$ (i.e., hydrogen is in excess). The same curve can be derived according to Eq. (6.6) assuming $E^{f_1}_{H_2O} - E^{f_2}_{H_2O} + E^{dec}_{OH} - E^{f}_{OH} = 0.07$ eV and $(1 - \theta_O)/\theta_O = 5$ (oxygen is in excess). This result demonstrates clearly that one route (in this example route (1.1)) may be dominant at high temperatures and the other at low temperatures.

This is illustrated in Fig. 9, which shows a change from route (1.1) dominating at high T to route (1.2) dominating at low T.

In summary, we found that the magnitudes of the activation energies of various steps of the hydrogen–oxygen reaction on Pt are such that it is very likely that one route is dominant at high temperatures and the other at low temperatures (Fig. 9), and that one route is dominant at hydrogen excess and the other at oxygen excess (see Fig. 10).

More accurate values of the activation energies for H_2O formation and OH formation and decomposition seem to be required to make firmer statements. A more detailed experimental and theoretical study of the temperature dependence of the OH desorption at different α-values (for instance by applying molecular beam relaxation spectroscopy (*31, 32*)) may help to discriminate between the two routes. In any case these observations seem to resolve the apparent contradiction in the literature that some investigations favor OH + H → H_2O and oth-

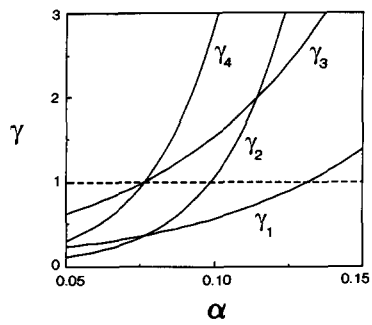

FIG. 10. The γ-value, defined in Eq. (6.6) as function of the relative hydrogen pressure, α, at $T = 1200$ K. The α-dependence of the oxygen coverage is determined by the expression given in Eq. (6.8), which is relevant in the α-region $0.05 < \alpha < 0.20$. γ is shown for different values of the energies $(E^{d}_{OH}, \Delta E)$, where $\Delta E = E^{f_2}_{H_2O} - E^{f_1}_{H_2O}$. Energies are given in eV. γ_1, (2.0, 0); γ_2, $(2.2 - B \cdot \theta_O, 0)$; γ_3, (2.0, 0.1); γ_4, $(2.2 - B \cdot \theta_O, 0.1)$, where $B = 0.7$ eV and θ_O is the oxygen coverage. The dashed line is drawn to indicate the crossover from reaction route (1.2) being dominant, $\gamma < 1$, to reaction route (1.1) being dominant, $\gamma > 1$.

ers OH + OH → H_2O + O as the water formation step. We think it is merely a matter of reaction conditions that determine which route dominates in a particular situation.

7. ENTHALPY DIAGRAM

The enthalpy diagram corresponding to the kinetic model was constructed using the following data. The O–Pt, H–Pt, and H_2O–Pt bond energies were taken from published data (Table 1), and the OH–Pt bond energy was derived as described in Sections 4 and 5 and in Ref. (*11*). Two values are shown for OH–Pt, 2.0 eV obtained using route (1.1), and 2.2 eV obtained using route (1.2) in the derivation. The diagram is representative of the high-temperature and zero coverage limits, where adsorbate–adsorbate interactions can be neglected. This is an important comment since the activation energies for O_2, H_2, and H_2O desorption, and thus the bond energies corresponding to Pt, are known to be coverage sensitive. It is likely that this applies to OH as well. Therefore the enthalpy diagram for the same reaction, but at low temperatures and high coverages, is expected to be different. This may be the reason that our enthalpy diagram differs from previously published diagrams. It may also explain the apparent contradiction between the relatively large activation energy for the $H_2O + O \rightarrow 2OH$ reaction in Fig. 5 and the experimental observations (*19*) that this reaction can proceed at temperatures well below room temperature when O is coadsorbed with H_2O. The latter experiments were performed at high coverages of H_2O and O and the enthalpy diagram is therefore modified by mutual interactions of H_2O, O, and OH.

How reliable is the enthalpy diagram shown in Fig. 5? It is consistent with the experimental results of Ljungström *et al.* (*10*) concerning OH and H_2O formation at steady state and high temperature. These are the data we aimed primarily at describing. The diagram also seems consistent with the results of Refs. (*3, 4, 13*) and, in fact, uses some of the information in those references. It must be emphasized, however, that closer analysis reveals an ambiguity. The analysis shows that our calculated data are sensitive to activation energy *differences* rather than to individual activation energies. For example, if we relax the assumptions (taken from Refs. (*3, 4, 13*) of 0.35 and 0.2 eV as upper limit values for the activation energies of the OH and H_2O formation steps, respectively, we find that reasonably good fits are obtained for route (1.2) as long as

$$2E^{d}_{OH}(0) - E^{f_2}_{H_2O} \approx 4.4\,\text{eV},$$

and for route (1.1) as long as

$$E^{d}_{OH}(0) - E^{f_1}_{H_2O} \approx 2.0\,\text{eV}.$$

This would then allow for considerably larger values of $E^{f_1}_{H_2O}$, $E^{f_2}_{H_2O}$, and $E^{d}_{OH}(0)$, still consistent with the data of Ref. (*10*) and with the measured E^{d}_{OH} values. It would also result in better agreement with the recently reported values by Anton and Cadogan (*31*): $E^{f}_{OH} = 0.6$ eV, $E^{d}_{OH} = 2.6$ eV, $E^{f_1}_{H_2O} =$

0.7 eV, $E^{f_2}_{H_2O} = 0.8$ eV. Remember, however, that a condition to obtain this latter agreement is that the overall activation energy for the H_2O formation reaction is allowed to be as high as 0.7 eV, in contrast to the results by the General Motors group (*3*) and others. The latter low-temperature results hardly allow a value larger than about 0.4 eV for either E^f_{OH} or $E^f_{H_2O}$. A value of 0.7 eV would, for example, give a net production rate of H_2O at 150 K of $\leq 10^{-11}$ H_2O per site per second. Since the low T-results are obtained at quite high coverages the 0.7 eV value obtained in the zero coverage limit could still be rationalized if adsorbate–adsorbate interactions lower the value to 0.4 eV at high coverage. At present there is not enough information to resolve this problem.

If we adopt an upper limit value of 0.4 eV for both E^f_{OH} and $E^f_{H_2O}$ the maximum acceptable value of $E^d_{OH}(0)$ consistent with the measured ε^d_{OH} and the overall kinetics are $E^d_{OH}(0) \leq 2.4$ eV, which is larger than the value reported in Ref. (*11*) (2.0 ± 0.15 eV) but still smaller than the recent value by Anton and Cadogan (2.6 eV). Obviously, measurements of the (coverage-dependent) activation energies E^f_{OH} and $E^f_{H_2O}$ are crucial for obtaining a more unique kinetic model and definitive values of $E^d_{OH}(\theta)$.

The exact magnitudes of the involved activation energies will of course also influence the relative importance of the OH + H → H_2O and OH + OH → H_2O + O steps for H_2O production at different α-values. With the values used in this work the first route (1.1) dominates at high temperatures at all α-values, except the very smallest. This was illustrated in Figs. 9 and 10. With the values of Ref. (*31*) the latter route (1.2) will, for example, dominate for most values $\alpha < \alpha_{H_2O}$ when the coverage dependence of E^d_{OH} is taken to be $B = 0.5$ eV in Eq. (2.14).

8. HIGH-PRESSURE LIMIT

The analytical expressions for the kinetics of water production presented in the previous sections are based on the assumption that the reaction is so fast that the surface is covered predominantly by oxygen for the oxygen excess region and almost empty when hydrogen is in excess. In this case, the rate of water production is proportional to the total pressure. The assumption is justified in the pressure and temperature regimes considered above. One would, however, expect that the kinetics of the hydrogen–oxygen reaction will change at sufficiently large total pressure or decreasing temperature so that this assumption is violated (e.g., when the impingement rates of H_2 and O_2 become comparable to or larger than the rate of the other reaction steps). Thus, it is of interest to analyze the reaction kinetics at high pressures beyond the regime where experimental data are available. An additional motivation for extrapolation of the reaction kinetics to high pressures is that the results obtained may be of value to guide future experiments in this P-regime and because such results may be of considerable interest for catalytic combustors (*30*).

The most important effect accompanying an increase in the total pressure is an increase in the hydrogen coverage. If we neglect oxygen and OH desorption and also the coverage dependence of the hydrogen sticking coefficient and assuming that route (1.1) is dominant (which is unproblematic for α-values $\geq \alpha_{H_2O}$), we have the following equations applicable at arbitrary hydrogen coverages (cf. Eqs. (3.4), (4.5), and (4.6))

$$2S_{O_2}(\theta)F_{O_2} + k^d_{H_2}\theta^2_H = S_{H_2}(0)F_{H_2} \quad (8.1)$$

$$r^f_{H_2O} = 2S_{O_2}(\theta)F_{O_2} = k^{f_1}_{H_2O}\theta_H\theta_{OH} \quad (8.2)$$

$$k^f_{OH}\theta_H\theta_O = k^{dec}_{OH}\theta_{OH}(1 - \theta). \quad (8.3)$$

Using these equations, one can analyze the effect of the total pressure on the reaction kinetics.

Considering, for example, α-values where the terms $S_{H_2}(0)F_{H_2}$ and $2S_{O_2}(0)F_{O_2}$ are of comparable magnitude but with hydrogen still in excess, we can easily obtain the following solution to Eqs. (8.1)–(8.3)

$$\theta_H \approx [S_{H_2}(0)F_{H_2}/k^d_{OH}]^{1/2} \quad (8.4)$$

$$\theta_O < k_{OH}^{dec} k_{H_2}^{d} / (k_{OH}^{f} k_{H_2O}^{f_1}) \quad (8.5)$$

$$\theta_{OH} \approx \theta_H k_{H_2}^{d} / k_{H_2O}^{f_1}. \quad (8.6)$$

The reaction is fast provided that

$$k_{OH}^{dec} k_{H_2}^{d} / (k_{OH}^{f} k_{H_2O}^{f_1}) \ll 1 \quad (8.7)$$

and

$$k_{H_2}^{d} / k_{H_2O}^{f_1} \ll 1. \quad (8.8)$$

Indeed, if conditions (8.7) and (8.8) are fulfilled, the surface is almost empty or predominantly covered by hydrogen.

A noticeable effect with increasing pressure is that the surface is eventually "poisoned" by hydrogen. At $T = 1000$ K, this hydrogen self-poisoning starts at $P \approx 10^4$ Torr. A key ingredient responsible for this result is that the coverage dependence of the sticking coefficient for oxygen is stronger than that for hydrogen, which favors H_2 adsorption when θ is large.

For the oxygen excess region the solution of Eqs. (8.1)–(8.3) is as follows (for simplicity, we write $\theta_O \approx 1 - \theta_O \approx 0.5$)

$$\theta_H \approx [S_{O_2}(\theta_O) F_{O_2} k_{OH}^{dec} / (k_{OH}^{f} k_{H_2O}^{f_1})]^{1/2} \quad (8.9)$$

$$\theta_{OH} \approx [S_{O_2}(\theta_O) F_{O_2} k_{OH}^{f} / (k_{OH}^{dec} k_{H_2O}^{f_1})]^{1/2}. \quad (8.10)$$

The reaction is fast if $\theta_H \ll 1$ and $\theta_{OH} \ll 1$. At $T = 1000$ K, this is the case when $P < 10^6$ Torr.

Finally, let us consider the case when $2S_{O_2}(0) F_{O_2} = S_{H_2}(0) F_{H_2}$ and the reaction rate is at its maximum. Using Eqs. (2.12) and (3.6) and assuming that the total coverage is low, we can rewrite Eqs. (8.1)–(8.3) as

$$4\theta S_{O_2}(0) F_{O_2} = k_{H_2}^{d} \theta_H^2 \quad (8.11)$$

$$2S_{O_2}(0) F_{O_2} = k_{H_2O}^{f_1} \theta_H \theta_{OH} \quad (8.12)$$

$$k_{OH}^{f} \theta_H \theta_O = k_{OH}^{dec} \theta_{OH}. \quad (8.13)$$

An elementary analysis of these equations shows that the hydrogen coverage becomes dominant with increasing pressure and we have

$$\theta_H \approx 2S_{H_2}(0) F_{H_2} / k_{H_2}^{d} \quad (8.14)$$

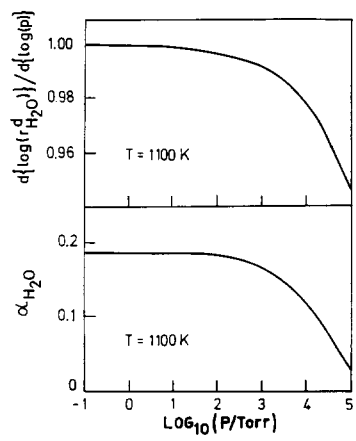

FIG. 11. The apparent order of H_2O desorption with respect to the total H_2 and O_2 pressures (upper panel) and the relative hydrogen concentration corresponding to the maximum water production (lower panel) as functions of log P. The results have been obtained by numerical solution of Eqs. (2.8)–(2.11) using the input parameters of Fig. 5 and Table 1.

$$\theta_O + \theta_{OH} \ll \theta_H. \quad (8.15)$$

Thus, the situation at the maximum H_2 production is about the same as that for hydrogen excess: the surface becomes "poisoned" by hydrogen with increasing total pressure. For example, if $T = 1000$ K, the poisoning starts at $P \approx 10^5$ Torr. This will cause the maximum in water production rate to shift to smaller α – values at sufficiently large pressure.

The analytical predictions presented in this section are in agreement with the results of the full numerical solutions of Eqs. (2.8)–(2.11). In particular, Fig. 11 shows the apparent order of the reaction and the relative hydrogen pressure near the maximum water production as a function of pressure at $T = 1100$ K. The effect of pressure on the apparent order and on α_{H_2O} is significant only at $P > 10^5$ Torr. The decrease in the apparent reaction order with increasing total pressure is accompanied by a decrease in α_{H_2O}. The reason for both these effects is that in this P-regime the surface coverage of hydrogen at $\alpha = \alpha_{H_2O}$ starts to be appreciable.

Experimental testing of the results at high P described in Fig. 10 is beset with appreciable difficulties. The very rapid kinetics at $T \sim 1000$ K would cause concentration gradients as P increases and the diffusion length becomes smaller and smaller with increasing P. It will be essentially impossible to maintain gradient-free conditions in the viscous flow regime at high temperatures. However, it may be possible to measure the mixing ratio for maximum H_2O production vs P, i.e., $\alpha_{H_2O}(P)$ and compare it with the calculated results of Fig. 11 (after correction for mass transport effects).

Concluding this section, we emphasize that quantitative extrapolation of the kinetics of heterogeneous reactions from one parameter region to another is known to be risky. An example illustrating this statement is the work by Zhdanov *et al.* (*6*) who studied the steady-state kinetics of the hydrogen–oxygen reaction on a Pt(111) surface at low (10^{-7}–10^{-6} Torr) and moderate (0.1–1.0 Torr) pressures for stoichiometric mixture of the reagents. The moderate-pressure kinetics were analyzed on the basis of data obtained in the transient studies at low pressures. It was found that the reaction rate, extrapolated from low to moderate pressures, exceeded the measured rate by about an order of magnitude. One of many phenomena that could influence the kinetics at high pressures is the presence of a predissociated state for hydrogen on the surface. Thus, extrapolation (*6*) has only yielded semiquantitative results. The same situation may be at hand in our case, and we therefore only emphasize the qualitative results of this section.

9. POSSIBLE MODEL IMPROVEMENTS

The model described above is relatively simple. It excludes a number of ingredients that one might expect to be important. For example, it seems well established that oxygen on Pt and Rh has a tendency to form islands, and that transient titration of adsorbed oxygen with hydrogen occurs preferentially at the boundaries of such islands (*2*). This could influence the kinetics both via the coverage dependence of hydrogen and oxygen sticking coefficients and of the intermediate reaction steps. In general, the island formation may be caused (i) by attractive lateral interactions between oxygen atoms, (ii) by the island mechanism of oxygen adsorption (adsorption occurs at the island boundaries), or (iii) if the titration reaction starts at the "active" sites and then islands are formed during the reaction process. The main reason that we did not need to take into account the island formation in this work is that the high temperatures considered are expected to randomize adsorbed oxygen on the surface. In other words at these high temperatures any mechanism of island formation is expected to be weak in comparison with thermal randomization.

Describing the reaction kinetics, we assumed that the surface is uniform. This assumption is partly justified because the surface of a well-annealed polycrystalline platinum is probably predominantly represented by the most close-packed plane, i.e., the (111) plane (*25*). The samples show upon inspection in SEM large crystallites >10–100 μm (*10*). On the other hand, it is not possible to exclude that the surface heterogeneity plays a role in the kinetics of the hydrogen–oxygen reaction, for example, in the kinetics of OH desorption. The possible effect of the surface heterogeneity on the latter process is discussed, for example, by Hsu *et al.* (*26*). More recently Verheij *et al.* (*32*) have directly demonstrated different reactivities of oxygen at step and terrace sites for OD formation on Pt(111).

One part of the model that may be improved in the future is the coverage dependences of the sticking coefficients. Lacking better knowledge, we have used $S_{O_2}(\theta) = S_{O_2}(0)(1 - \theta)^2$, as suggested by experiments at lower temperatures (*17*), and $S_{H_2}(\theta) = S_{H_2}(0)$. It is quite likely that these expressions need to be refined, e.g., that the hydrogen sticking on an oxygen saturated surface is different from $S_{H_2}(0)$. Also, the

structural state of the surface (step density, etc.) are known to influence both O_2 and H_2 sticking on Pt. To extend the validity regime of the model, more refined rate constants should be included, e.g., T-dependent pre-exponential factors, coverage-dependent activation energies (when available from experiments), and so on.

As a general conclusion, improvements of the model must await further experiments over a larger range of pressures and temperatures and on single-crystal samples at higher pressures and temperatures than those in previous studies. Concerning the enthalpy diagram and activation energies, there are considerable improvements to be made in the activation energies E^{f}_{OH}, $E^{f_1}_{H_2O}$ and $E^{f_2}_{H_2O}$. Low-temperature experiments of the type described by Germer and Ho (*13*) using time-resolved EELS to follow the time evolution of OH (and H_2O) during H_2 dosing of an oxygen-precovered Pt surface are very promising in this respect as are molecular beam relaxation spectroscopy (MBRS) measurements (*31, 32*). Further kinetic measurements of OH and H_2O production at high temperatures will be important, as will studies of OH production in the $H_2O + \frac{1}{2}O_2 \rightarrow OH + OH$ reaction on Pt and possibly also studies of the water decomposition reaction $H_2O \rightarrow OH + H$.

10. SUMMARY

We have constructed a kinetic model to describe the rates of water and hydroxyl desorption during the hydrogen–oxygen reaction on Pt at high temperatures, ~1000 K, and pressures primarily in the range up to 0.1 Torr. The model is based on dissociative H_2 and O_2 sticking and hydrogen addition to O to form OH. Two different routes for water formation were considered, viz., $H + OH \rightarrow H_2O$ and $OH + OH \rightarrow H_2O + O$. The model takes into account decomposition of OH to O + H. Inclusion of the latter process is important in order to obtain agreement with experiments. An enthalpy diagram for the reaction has been constructed on the basis of the calculations and available experimental data. The kinetic equations for various steps have been derived assuming that the surface is uniform, and that adsorbed species are randomly distributed.

If the temperature is kept fixed, both routes of the H_2O formation reaction have been shown capable of yielding a good quantitative description of the OH and H_2O desorption rates as functions of gas mixture and pressure in the regimes where experimental data are available. The hydrogen addition reaction gives good agreement with no or small coverage dependence of the activation energy for OH desorption while the $OH + OH \rightarrow H_2O + O$ route can account for the experimental data only if a considerable lowering of the OH desorption energy with increasing oxygen coverage is assumed. The temperature dependence of the OH desorption is reproduced better by the first route ($OH + H \rightarrow H_2O$). This route is concluded to be dominant in the hydrogen–oxygen reaction at least at high temperatures and not too large an oxygen excess. However, the results also demonstrate that transitions are likely from one dominating route to the other as the temperature and/or the H_2/O_2 ratio are varied.

It is concluded that a unique enthalpy diagram for the $H_2 + O_2$ reaction on Pt is still lacking, even at zero coverage. Adsorbate–adsorbate interactions are expected to modify the enthalpy diagram at high coverages.

The model has been used to predict the reaction kinetics at pressures as high as 10^5 Torr. These results may be useful as guides to high-pressure experiments and in calculations of catalytic combustor performance.

APPENDIX

The steady-state equations (2.8)–(2.11) can be written in a closed vector form

$$\mathbf{f} = 0, \qquad \text{(A1)}$$

where $\mathbf{f} = (f_1, \ldots, f_M)$. The f_i's are coverage dependent functions and M is the dimensionality of the problem (the number of rate equations, e.g., the number of surface cov-

erages to be calculated). The set of nonlinear coupled equations (A1) can be solved using the multidimensional Newton–Raphson (NR) method (*29*) as follows. A grid of N points, including the end points, is set for the α-parameter (α is the relative hydrogen pressure), $\alpha_n = n\Delta$, where $N - 1 > n > 0$ and $\Delta = (N - 1)^{-1}$. The solution of the rate equations is found successively, starting from $n = 0$ and further increasing α with Δ until $n = N - 1$. For $\alpha_0 = 0$ an analytical solution for the coverages $\Theta_0 = (\theta_H, \theta_O, \theta_{OH}, \theta_{H_2O})_0$ is easily found. The coverages Θ_1 for $\alpha_1 = \Delta$ is then solved iteratively with Θ_0 as a first guess, and so on. The general iterative NR procedure to be carried out for each α-value, is given by

$$\Theta^{(i+1)} = \Theta^{(i)} - D^{(i)}\mathbf{f}^{(i)}, \qquad \text{(A2)}$$

where $D = J^{-1}$ and $[J]_{r,m} = \partial f_r/\partial\theta_m$. According to Eq. (A2), the matrix D, defined as the inverse of the Jacobian matrix, J, must be recalculated in each iteration step. In our case, when M is rather small ($M = 4$), the method is very fast and accurate. In the pressure and temperature range of consideration, typically $N = 300$ and $N_i = 10$ (number of iterations) is sufficient.

ACKNOWLEDGMENTS

We thank E. Fridell and K. E. Keck for many valuable discussions on the H_2O and OH kinetics, and G. Wahnström for sharing his knowledge about surface diffusion of hydrogen on metals. We are also grateful to Brad Anton, Cornell University, for enlightening discussions and private communication of experimental data and their analysis, prior to publication. Financial support was obtained from the National Swedish Board for Technical Development (STU Contracts No. 83-5404 and No. 83-05405P), from the Swedish Natural Science Research Council (NFR, Contract E-EG 2560-129) and from National Energy Administration (STEV, Contract No. 246 003). One of us (V.P.Z) also thanks the Royal Swedish Academy of Sciences for supporting his visit to Chalmers University of Technology.

REFERENCES

1. Norton, P. R., *in* "The Chemical Physics of Solid Surfaces and Heterogeneous Catalysis" (D. A. King and D. P. Woodruff, Eds.), Vol. 4, p. 70. Elsevier, Amsterdam, 1982.
2. Gland, J. L., Fisher, G. B., and Kollin, E. B., J. Catal. **77,** 263 (1982).
3. Fisher, G. B., Gland, J. L., and Schmieg, S. J., J. Vac. Sci. Technol. **20,** 518 (1982).
4. Ogle, K. M., and White, J. M. Surf. Sci. **139,** 43 (1984).
5. Zhdanov, V. P., Surf. Sci. **169,** 1 (1986).
6. Zhdanov, V. P., Sobolev, V. I., and Sobyanin, V. A., Surf. Sci. **175,** L747 (1986).
7. Hellsing, B., Kasemo, B., Lungström, S., Rosén, A., and Wahnström, T., Surf. Sci. **189/190,** 851 (1987).
8. Hall, J., Kasemo, B., Ljungström, S., Rosén, A., and Wahnström, T., J. Vac. Sci. Technol. **A5,** 523 (1987).
9. Hellsing, B., and Kasemo, B., Chem. Phys. Lett. **148,** 65 (1988).
10. Ljungström, S., Kasemo, B., Rosén, A., Wahnström, T., and Fridell, E., Surf. Sci. 216, 63 (1989).
11. Wahnström, T., Fridell, E., Ljungström, S., Hellsing, B., Kasemo, B., and Rosén, A., Surf. Sci. Lett. **223,** L905 (1989).
12. Mitchell, G. E., and White, J. M., Chem. Phys. Lett. **135,** 84 (1987).
13. Germer, T., and Ho, W., Chem. Phys. Lett. **165,** 449 (1989).
14. Zhdanov, V. P., Surf. Sci. **209,** 523 (1989); **219,** L571 (1989); J. Phys. Chem. **93,** 5582 (1989).
15. Zhdanov, V. P., and Hellsing, B., unpublished results.
16. Zhdanov, V. P., Pavlicek, J., and Knor, Z., Catal. Rev. Sci. Eng. **30,** 501 (1988).
17. Campbell, C. T., and Ertl, G., Kuipers, H., and Segner, J., Surf. Sci. **107,** 220 (1981).
18. Fisher, G. B., and Gland, J. L., Surf. Sci. **94,** 446 (1980).
19. Fisher, G. B., and Sexton, B. A., Phys. Rev. Lett. **44,** 683 (1980); Stuve, E. M., Madix, R. J., and Sexton, B., Surf. Sci. **111,** 11 (1981); Ollé, L., Salmerón, M., and Baró, A. M., J. Vac. Sci. Technol. **A3,** 866 (1985); Hock, M., Seip, U., Bassignana, I., Wagemann, K., and Kuppers, J., Surf. Sci. **177,** L978 (1986); Gurney, B. A., and Ho, W., J. Chem. Phys. **87,** 5562 (1987).
20. Norton, P. R., Davies, J. A., and Jackman, T. E., Surf. Sci. **121,** 103 (1982).
21. Nieuwenhuys, B. E., Surf. Sci. **126,** 307 (1983).
22. This value corresponds to the activation energy for the overall water reaction, determined by Fisher *et al.* (*3*).
23. Private communication with T. Wahnström *et al.* (see Ref. (*10*). These recent, experimentally determined values differ slightly from the ones given earlier (*10*) $S_{H_2}(0) = 0.04$ and $S_{O_2}(0) = 0.02$.
24. Nyberg, C., and Tengstål, C. G., J. Chem. Phys. **80,** 3463 (1984); Nyberg, C., and Uvdal, P., J. Chem. Phys. **84,** 4631 (1986).

25. Shigeishi, R. A., and King, D. A., Surf. Sci. **58,** 379 (1976).
26. Hsu, D. S. Y., Hoffbauer, M. A., and Lin, M. C., Surf. Sci. **184,** 25 (1987).
27. (a) Seebauer, E. G., and Schmidt, L. D., Chem. Phys. Lett. **123,** 129, (1986); (b) George, S. M., DeSantolo, A. M., and Hall, R. B., *Surf. Sci.* **159,** L425 (1985); Mullins, D. R., Roop, B., Costello, S. A., and White, J. M., *Surf. Sci.* **186,** 67 (1987).
28. Zhdanov, V. P., unpublished results.
29. Dahlquist, G., and Björk, Å, "Numerical Methods," p. 248, Prentice Hall, Englewood Cliffs, NJ, 1974.
30. Griffin, T. A., Ph.D. thesis, Department of Chemical Engineering, Yale University, New Haven, CT, 1989.
31. Anton, A. B., and Cadogan, D. C., Surf. Sci. Lett. **239,** L548 (1990).
32. Verheij, L. K., Hugenschmidt, M. B., Cölln, L., Poelsema, B., and Comsa G., *Chem. Phys. Lett.* **166,** 523 (1990).
33. E. Fridell, M.Sc. Thesis, Chalmers Univ. Techn., 1990.